Review

A Comprehensive Review of Thermoelectric Generators from Micropower Supply to Kilowatt System

Shuo Yang, Hao Chen and Ding Luo *

Shaanxi Key Laboratory of New Transportation Energy and Automotive Energy Saving, Chang'an University,
Xi'an 710064, China
* Correspondence: Ding_L@outlook.com

Abstract: Energy crisis and carbon emissions are two increasingly prominent issues in our society. As one of the clean energy sources, thermoelectric power generation is a promising alternative energy technology to convert heat into electricity. As long as there is a heat source, thermoelectric generators can provide electricity for watches, sensors, electronics, spacecraft, etc., and can also be used to recover waste heat, such as automobile exhaust heat, industrial waste heat, ship waste heat, etc. This study proposes a novel classification paradigm based on power output (microwatt, 1 W–1 kW, >1 kW), systematically revealing the technological characteristics at each power level: the microwatt level relies on flexible materials and compatibility with human body heat, while the kilowatt level requires the integration of high-temperature materials and optimized thermal management. The study also demonstrates that performance can be significantly enhanced through asymmetric geometric designs and non-equilibrium synthesis processes. This work provides a comprehensive design framework, from material innovation to large-scale integration, for next-generation thermoelectric systems, addressing the theoretical gap in techno-economic analysis.

Keywords: thermoelectric generators; waste heat recovery; kilowatt; thermal management

1. Introduction

In recent years, fossil fuel consumption and carbon emissions caused by electricity production have been the focus of the whole society. Many countries have issued policies to reduce the use of primary energy and promote renewable energy development. The proportion of renewable energy in global electricity production is gradually increasing, as shown in Figure 1. The development of renewable energy has attracted great interest from researchers. As one of the renewable energy, thermoelectric power generation has incomparable advantages over other clean energy, such as, no moving component, no noise, weather independence, simple structure, no maintenance cost, long life, and so on [1–4], which has the potential to become a promising alternative energy technology.
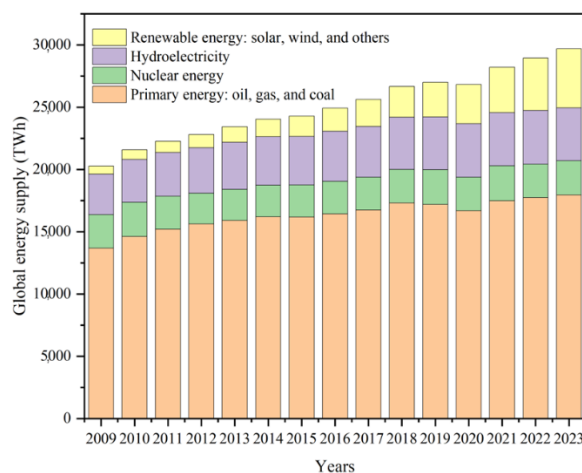

Figure 1. Global electricity production with different sources.

Thermoelectric generators (TEGs) can directly transfer heat into electricity when there is a temperature difference on both ends of TEGs. Various types of heat energy can be used to generate electricity by different TEG systems [5]. According to the different heat sources, the power generation level of TEG systems is quite different, from micro power supply to kilowatt system. Some preliminary TEG applications have been witnessed. The wearable TEG device can harvest body heat to provide power for watches or other electronics [6]. In space exploration, the spacecraft driven by the photovoltaic (PV) power supply does not work without light, which affects the normal progress of the exploration mission; The radiative TEG system can overcome the impact of the environment and continue to provide power, and NASA has started the relative research plan since 1951 [7]. To further enhance the efficiency of PV semiconductors, thermoelectric materials can be combined with PV materials to form a PV-TEG device, which can use both solar and thermal energy [8]. Zhao et al. [9] enhanced the efficiency of a photovoltaic-thermoelectric generator (PV-TEG) by integrating microchannel heat pipes and phase change materials; They further applied a hybrid optimization algorithm to perform multi-objective optimization on the system, achieving a remarkable electrical efficiency of 25.6% for the PV-TEG. Considering that about 1/3 of energy produced by burning fossil fuels is wasted in the form of exhaust heat, the automobile TEG system can be installed in the vehicle exhaust system to convert the exhaust heat into electricity and improve fuel efficiency [10–14]. Also, the thermoelectric power generation technology can be applied to recover other forms of waste heat, such as industrial waste heat [15], ship waste heat [16], etc. For instance, Zhuang et al. [17] conducted an in-depth numerical simulation study on industrial thermal environments and heat transfer characteristics of TEGs, thereby developing a novel industrial waste heat recovery TEG system that combines high power generation efficiency with operational stability. Innovatively, Li et al. [18] introduced a radiation shielding layer within the thermoelectric leg gaps, which effectively reduced heat loss and enhanced system conversion efficiency and output power by 15% and 9.5%, respectively. There is an increasing interest in thermoelectric power generation technology.

However, the TEG has not yet been widely commercialized due to its relatively low conversion efficiency and high cost of thermoelectric materials. The ability of the TEG to convert heat energy into electricity depends on the performance of thermoelectric materials, which is estimated by a dimensionless constant of figure-of-merit $ZT = \sigma\alpha^2 T\lambda^{-1}$, wherein σ is the electrical conductivity, α is the Seebeck coefficient, T is the absolute temperature, and λ is the thermal conductivity [19,20]. At present, Bi_2Te_3-based materials are the only commercialized thermoelectric materials because of the relatively high ZT value near room temperature, about 1. The ideal conversion efficiency of the TEG can be estimated by the ZT value, that is

$$\eta = \frac{T_h - T_c}{T_h} \frac{\sqrt{1 + ZT} - 1}{\sqrt{1 + ZT} + \frac{T_c}{T_h}} \tag{1}$$

where T_h and T_c are the hot-side and cold-side temperatures, respectively. Figure 2 shows the conversion efficiency of the TEG with different ZT values as well as the comparison with Carnot efficiency. In numerous application scenarios, such as automotive waste heat recovery, a temperature difference of 150 K can be easily achieved. When the ZT value exceeds the threshold value of 2 [20,21], the conversion efficiency can reach more than 10%, and the application of the TEG will become more competitive compared with other alternative energy conversion technologies such as the PV energy conversion. Researchers aim to identify thermoelectric materials with a ZT value of 2.0 using advanced material technologies.

With the progress of thermoelectric materials, an increasing number of thermoelectric power generation systems have been reported in different industries. TEG systems with different power generation levels feature different barriers that block their wide applications. For example, the micro power supplies, such as wearable TEG devices and self-powered sensors, need to satisfy the requirement of flexible structures to adapt to different heat source shapes. Kilowatt TEG systems require a heat exchanger with good heat transfer performance to improve the hot-side work temperature and a good electrical connection scheme to reduce the parasitic power losses. In the previous work, we provided a comprehensive review of thermoelectric technology, from materials to systems [22]. The thermoelectric applications were also reviewed and summarized [23]. As the development of TEG systems continues to flourish, new challenges emerge in different scenarios, thus a more recent and classified review is required.

In this review, TEG systems are classified according to different power generation levels. Section 2 introduces the basics of the TEG, including thermoelectric effects, thermoelectric materials, and the TEG design. Section 3 presents the development of thermoelectric micropower supplies. Section 4 comprehensively reviews TEG systems from 1 W to 1 kW. Section 5 introduces the application of TEGs in power generation systems that exceed 1 kW. The challenges and outlook for TEG systems are also discussed.
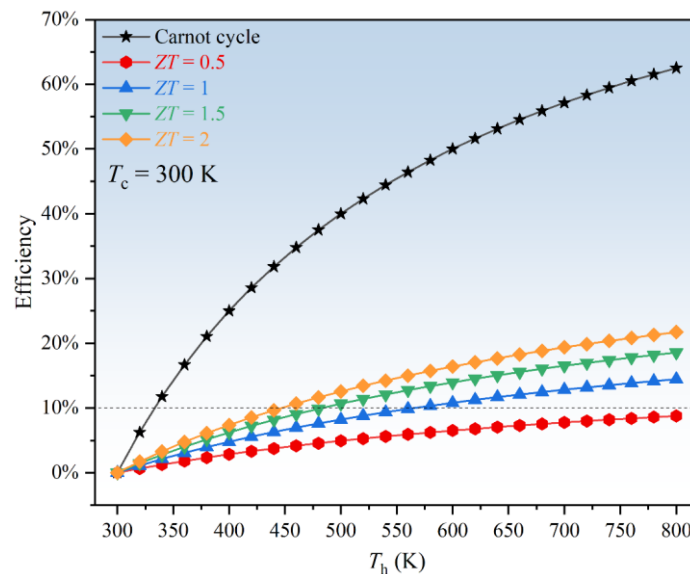
Figure 2. The conversion efficiency of the TEG with different *ZT* values.

2. Basics of the Thermoelectric Generator

As the basic power source of thermoelectric power generation systems, the TEG is composed of p- and n-type thermoelectric legs, metal connectors, and insulating plates, and presents a sandwich configuration, as shown in Figure 3. When the heat source applies a heat flux to one side of the TEG, the high temperature will induce the movement of the holes on p-type thermoelectric legs and the electrons of n-type thermoelectric legs towards the side with lower temperature, and the heat will be dissipated by a cooling source attached on the other side of the TEG. Multiple thermocouple pairs, connected in series, can amplify the voltage, and the current is produced once an external load is connected. This device has no mechanical moving parts and can generate power from heat sources such as industrial waste heat, automobile exhaust, or radioisotopes. The p- and n-type thermoelectric legs are connected electrically in series and thermally in parallel. To reduce parasitic power loss, metal connectors, usually made of copper, must have high thermal and electrical conductivity. To increase the temperature difference on both sides of the TEG, insulating plates possess high thermal conductivity [24] and are usually made of ceramics. The performance of AIN ceramic plate is better than Al_2O_3 based ceramic plate, but the cost is higher.
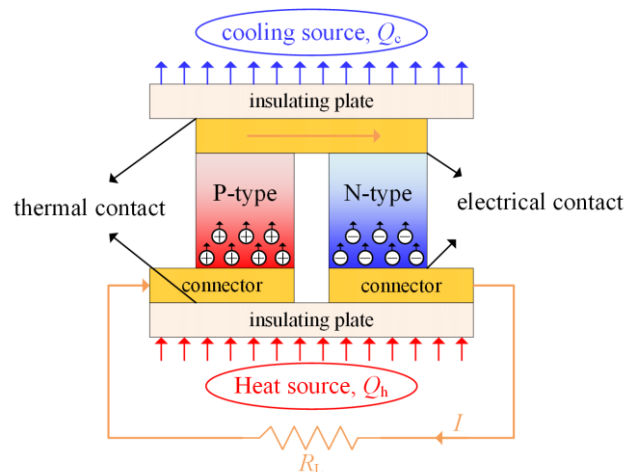

Figure 3. A diagram showing the working principle of the TEG.

2.1. Thermoelectric Effects

Thermoelectric effects include Seebeck, Peltier, and Thomson effects. The Seebeck effect was first discovered by Thomas Seebeck in 1821. When different conductors (or semiconductors) are connected and subjected to a temperature gradient, the Seebeck voltage will be generated. The Seebeck voltage is directly proportional to the Seebeck coefficient and temperature difference, which can be estimated by:

$$V = \alpha \Delta T \tag{2}$$

where α is the Seebeck coefficient, and ΔT is the temperature difference. Therefore, thermoelectric materials must have a high Seebeck coefficient to produce considerable voltage.

The Peltier effect, a fundamental aspect of the thermoelectric effect, can be considered the reverse of the Seebeck effect. First discovered by Jean Peltier in 1834, it involves the reversible conversion of electrical and thermal energy. When an external current I flows through a thermocouple made of two distinct conductor or semiconductor materials (A and B), Peltier heat is produced at the junction, alongside the Joule heating due to resistance. Peltier heat is generated at both ends of thermoelectric legs, wherein the end of carrier accumulation will release heat and the end of carrier dissipation will absorb heat. The amount of Peltier heat can be expressed as:

$$Q_{Peltier} = \pi I = \alpha I T \tag{3}$$

where π is the Peltier coefficient. Peltier coefficient and Seebeck coefficient are closely related through Kelvin relation, i.e., $\pi = \alpha T$. Due to the Peltier effect, thermoelectric materials were also used to fabricate thermoelectric coolers for cooling electronic devices [25].

The Thomson effect, discovered by William Thomson in 1854, describes a unique thermal phenomenon in a homogeneous material when both a temperature gradient and an electric current are present. When current flows through a thermoelectric material with a temperature gradient, the carriers generate additional heat due to changes in their kinetic energy (Thomson heat). If the current direction aligns with the temperature gradient, the material releases heat; otherwise, it absorbs heat. Thomson heat is directly proportional to the current and temperature gradient, which can be estimated by:

$$Q_{Thomson} = \tau I \Delta T \tag{4}$$

where τ is the Thomson coefficient. The Thomson coefficient τ is related to the temperature dependence of the Seebeck coefficient ($\tau = T\frac{d\alpha}{dT}$). Although the effect is weak, the directional sensitivity endows it with a unique value in dynamic temperature control scenarios.

In the global heat transfer process of thermoelectric legs, there are four kinds of heat: heat conduction, Peltier heat, Joule heat, and Thomson heat. The relationship among them is that the heat conduction is the largest, followed by Peltier heat, Joule heat, and Thomson heat [26].

2.2. Thermoelectric Materials

With the development of semiconductor physics, more and more ideal thermoelectric materials have been found, among which thermoelectric materials synthesized by tellurium (Te), bismuth (Bi), antimony (Sb), or selenium (Se) are the conventional Bi_2Te_3-based materials for the preparation of TEGs [27]. Owing to the modern synthesis and characterization techniques, conventional bulk thermoelectric materials with nanostructures have thrived, such as nanostructured Bi_2Te_3 [28], PbTe [29], and SiGe [30], and the *ZT* value has been improved to a certain extent. In addition to conventional thermoelectric materials, skutterudite, half-Heusler, and organic thermoelectric materials have also been widely used in different application scenarios. Based on the different working temperatures, thermoelectric materials are classified into three categories: low- (300–500 K), medium- (500–900 K), and high-temperature (>900 K) materials. Low-temperature thermoelectric materials mainly include Bi_2Te_3 and organic materials, medium-temperature thermoelectric materials mainly include PbTe and skutterudite, and high-temperature thermoelectric materials mainly include SiGe and half-Heusler. In recent years, with the continuous advancement in thermoelectric materials research, various novel thermoelectric materials have been developed to significantly enhance thermoelectric performance. This section systematically reviews and discusses recent research progress in the field of thermoelectric materials.

In the field of low-temperature thermoelectric materials, Kim et al. [31] developed a cost-effective synthesis strategy for Bi_2Te_3-based thermoelectric materials, as illustrated in Figure 4a. This technique employs rapid extrusion of excess liquid during the pressing process, significantly enhancing thermoelectric performance in bismuth telluride (Bi_2Te_3) specimens. The proposed methodology effectively circumvents electrical conductivity degradation through the strategic introduction of grain boundary dislocations, ultimately achieving a peak *ZT* value of 1.86 at 320 K. Wang et al. [32] effectively suppressed Te vacancies in n-type nanostructured Bi_2Te_3 through spark plasma sintering (SPS)-induced non-equilibrium reactions, as demonstrated in Figure 4b. This approach remarkably reduced thermal conductivity to 0.48 W·m^{-1}·K^{-1} while maintaining a *ZT* value of 1.1 at 420 K in the thermoelectric leg. Meroz et al. [33] demonstrated an optimized synthesis protocol for n-type $Bi_2Te_{2.4}Se_{0.6}$ by integrating the melt spinning technique with hot pressing; This hybrid processing strategy yielded a maximum *ZT*

value of 1.07 at 338.15 K, showcasing enhanced thermoelectric performance through combinatorial fabrication approaches. Zheng et al. [34] proposed a design scheme for a full-scale hierarchical structure (Figure 4d). This scheme achieved multiple scattering of phonons by introducing a high density of grain boundaries, dislocations, layer dislocations, twin boundaries and nanoholes, which significantly reduced the lattice thermal conductivity of the MgAgSb material over the entire temperature range. The thermoelectric material achieved a *ZT* value of 1.4.
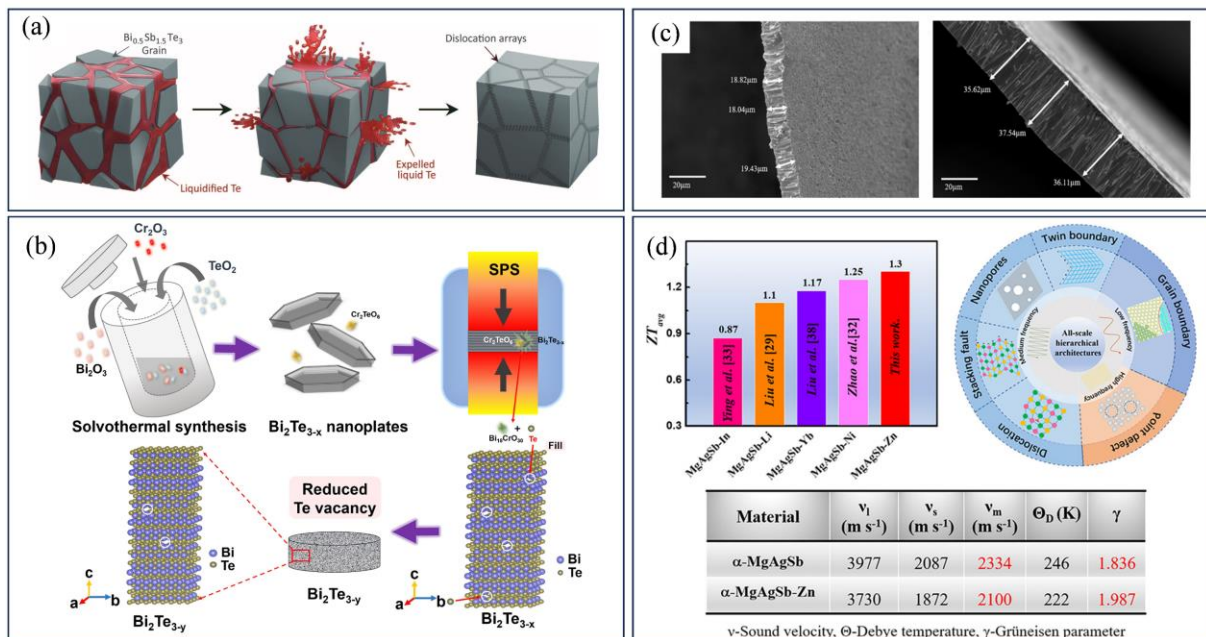

Figure 4. (**a**) Schematic illustration showing the generation of dislocation arrays during the liquid-phase compaction process. "Reprinted with permission from Ref. [31].2015, Kim, S.I."; (**b**) Non equilibrium reaction induced by spark plasma sintering. "Reprinted with permission from Ref. [32]. 2020, Wang, Y."; (**c**) SEM cross-sectional micrograph of $Bi_2Te_{2.4}Se_{0.6}$ thin films after melt spinning at 600 and 300 rpm. "Reprinted with permission from Ref. [33]. 2020, Meroz, O."; (**d**) A design scheme of full-scale hierarchical structure. "Reprinted with permission from Ref. [34]. 2019, Zheng, Y.".

Research on medium- and high-temperature thermoelectric materials have achieved significant breakthroughs. Wu et al. [35] proposed an innovative strategy involving alternating regulation of interatomic interactions through lattice strain modulation while maintaining the original material composition. This methodology achieved a remarkable 58% reduction in lattice thermal conductivity without sacrificing carrier mobility, ultimately realizing an exceptional *ZT* value of 2.6 at 850 K in the engineered material system. Rogl et al. [36] successfully synthesized (R_0) with a nominal composition of $(R_{0.33}Ba_{0.33}Yb_{0.33})_{0.35}Co_4Sb_{12.3}$ (R = Sr, La, DD, MM, SRMM, SRDD) massive n-type three filled and multi filled skutterudite materials. The experimental results show that the series of thermoelectric materials achieve the highest *ZT* value of 1.8 at 835 K. Tsai et al. [37] significantly reduced the thermal conductivity of the material by introducing Sb_2Te_3 alloying into GeTe-based thermoelectric materials, while maintaining a suitable carrier concentration over a wide compositional range. Owing to this optimization strategy, the material can achieve a *ZT* value > 2.6 at 720 K. Saiga et al. [38] systematically investigated the effect of Cu doping on $Ba_8Ga_{16}Sn_{30}$ crystal growth and its thermoelectric properties. The results show that the *ZT* values of p-type and n-type single crystals reach 0.88 and 1.45 at 520 K, respectively, with the n-type single crystals having the highest *ZT* values among all the substitution systems of $Ba_8Ga_{16}Sn_{30}$. Shi et al. [39] successfully optimized the synergistic optimization of high carrier concentration and mobility in n-type Mg_3Sb_2 alloys by introducing Y doping at the cationic position. It was found that the material's thermoelectric properties were significantly better than those of the previously reported n-type Mg_3Sb_2 system, achieving a *ZT* value as high as 1.8 at 700 K.

In different application scenarios, variations in operating temperature range cause significant differences in the thermoelectric material systems used. For example, micropower supplies typically operate in the low-temperature range, TEG systems in the 1 W to 1 kW order of magnitude are mostly deployed in the low or medium-temperature range, and TEG systems with power levels greater than 1 kW need to be matched to medium- or high-temperature operating environments. Table 1 systematically summarizes the peak *ZT* values of thermoelectric materials and their corresponding temperature regions in the above studies. Therefore, temperature matching and

material selection based on actual working conditions are of great significance for optimizing system performance, and key factors such as thermal stability of materials, temperature dependence of thermoelectric parameters, and interfacial compatibility need to be considered comprehensively.

Table 1. Optimum *ZT* values and operating temperatures of various thermoelectric materials.

Materials	Type	*ZT* Value	Temperature	Ref.
$Bi_{0.5}Sb_{1.5}Te_3$	p-type	1.86	320 K	[31]
$Bi_2Te_{2.86}$	n-type	1.1	420 K	[32]
$Bi_2Te_{2.4}Se_{0.6}$	n-type	1.07	338 K	[33]
$Mg_{0.97}Zn_{0.03}Ag_{0.9}Sb_{0.95}$	p-type	1.4	423 K	[34]
$Na_{0.03}Eu_{0.03}Sn_{0.02}Pb_{0.92}Te$	p-type	2.6	850 K	[35]
$(R_{0.33}Ba_{0.33}Yb_{0.33})_{0.35}Co_4Sb_{12.3}$	n-type	1.8	835 K	[36]
$(GeTe)_{0.95}(Sb_2Te_3)_{0.05}$	p-type	2.7	720 K	[37]
$Ba_8Ga_{16}Sn_{30}$	n-type	1.45	520 K	[38]
$Mg_{3.05-x}Y_xSbBi$	n-type	1.8	700 K	[39]

2.3. Design of the Thermoelectric Generator

Conventional TEGs typically employ symmetric cubic configurations for their thermoelectric semiconductors, as depicted in Figure 5a, where p-type and n-type thermoelectric legs maintain identical geometric dimensions. However, research has shown that geometric optimization of thermoelectric components, including asymmetric architectures and gradient cross-sections, can enhance performance. This structural optimization enables precise regulation of heat flux distribution, enhanced phonon scattering mechanisms, and minimized interfacial thermal losses, thereby establishing novel design paradigms for high-efficiency TEG systems. Luo et al. [40] proposed an L-shaped TEG configuration (Figure 5b) accounting for inherent material parameter disparities between p-type and n-type thermoelectric materials. This innovative configuration engineer's distinct height dimensions for p-type and n-type semiconductor legs. Experimental results demonstrate that under a temperature difference of 400 K, the L-shaped TEG yielded a maximum output power of 1.96 W with a conversion efficiency of 7.8%, representing 2.39% and 1.44% enhancements, respectively, compared to conventional π-type TEG counterparts. Wang et al. [41] proposed an X-type TEG configuration (Figure 5c) and systematically analyzed its thermoelectric and mechanical properties under steady-state conditions. The results show that under the temperature difference of 200 K, the maximum output power of the X-type thermoelectric module reaches 0.0847 W, and the conversion efficiency is 5.2%, which is about 4.57% higher than the traditional configuration. Luo et al. [42] proposed a ring-shaped TEG configuration with variable cross-sectional area (Figure 5d), in which the cross-sectional area of thermoelectric legs increases along the gradient of heat flow direction to alleviate the performance degradation caused by the decline of temperature gradient. The results show that the output power of the annular TEG is 76.66 W, and the conversion efficiency is 1.45%, which is 8.97% and 8.93% higher than the traditional configuration, respectively.

In addition, the two-stage TEG further improves the comprehensive performance of TEG by stacking two thermoelectric modules up and down. Enciso-Montes et al. [43] proposed a two-stage TEG configuration (Figure 5e) and systematically studied the influence of different thermoelectric leg shapes on TEG performance. The results show that although the efficiency of two-stage TEG and single-stage TEG is 3.9%, the peak voltage of two-stage TEG is 97.6 mV, which is significantly higher than that of single-stage TEG of 49.7 mV. Bian et al. [44] developed a two-stage TEG configuration (Figure 5f), in which different thermoelectric materials are used at the hot end and cold end to adapt to the corresponding temperature range. In this study, the non-dominated sorting genetic algorithm II (NSGA-II) was introduced for the first time to optimize TEG's electrical output performance and mechanical stability.

Considering the different optimal working temperatures of different thermoelectric materials and the temperature gradient of thermoelectric legs from the hot side to the cold side, the segmented design can effectively overcome the negative impact of the temperature drop, in which the high-temperature area adopts high- or medium-thermoelectric materials and the low-temperature area adopts medium- or low-temperature thermoelectric materials. Zhang et al. [45] prepared a Bi_2Te_3/Skutterudite segmented thermoelectric module (Figure 5g), and achieved a conversion efficiency of up to 12% at a temperature difference of 541 K, setting a record in the field, with an output power of 5.6 W. He et al. [46] developed a double-cone segmented thermoelectric generator (Figure 5h). The results show that, compared with the traditional segmented ring thermoelectric generator, the output power of the double cone segmented ring thermoelectric generator is increased by 20.23%, the energy efficiency is increased by 8.55%, and the economic cost is reduced by 21.36%. Sun et al. [47] combined the multi-objective genetic algorithm with the finite element method to optimize the multi-parameter and multi-objective of the segmented

annular TEG. The results show that the optimized segmented TEG has an output power of 0.04326 W and an efficiency of 9.63% at a temperature difference of 300 K, which is 32.839% and 61.915% higher than that before optimization, respectively.
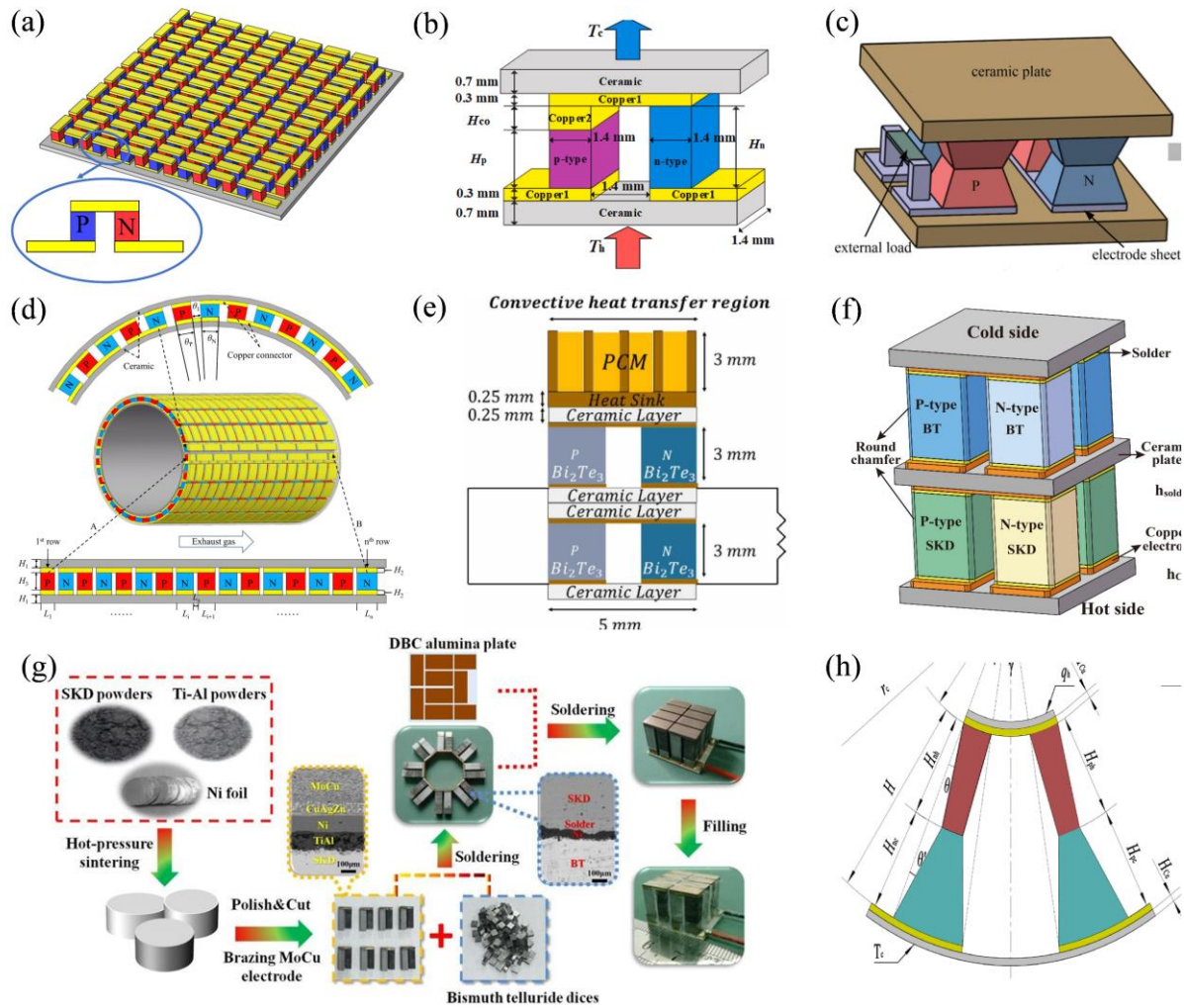

Figure 5. (**a**) Traditional π-type TEG; (**b**) L-type TEG. "Reprinted with permission from Ref. [40]. 2024, Luo, D."; (**c**) X-type TEG. "Reprinted with permission from Ref. [41]. 2020, Wang, R."; (**d**) Variable cross-sectional area annular TEG. "Reprinted with permission from Ref. [42]. 2024, Luo, D."; (**e**) Two-stage TEG. "Reprinted with permission from Ref. [43]. 2024, de Oca, O.Y.E.-M."; (**f**) Two-stage TEG with different thermoelectric materials between the upper and lower stages. "Reprinted with permission from Ref. [44]. 2025, Bian, M."; (**g**) Bi$_2$Te$_3$/Skutterudite segmented TEG. "Reprinted with permission from Ref. [45]. 2017, Zhang, Q."; (**h**) Biconical segmented annular TEG. "Reprinted with permission from Ref. [46]. 2024, He, H".

Table 2 summarizes the above studies. Based on the review and analysis of the TEG design strategy, it can be seen that the thermoelectric performance of TEG can be significantly improved through effective structural design (such as asymmetric configuration, segmented integration, multi-objective optimization, etc.). These design strategies provide important theoretical guidance and technical path for realizing high-performance TEG by optimizing heat flow distribution, interface contact resistance and electrical transport characteristics.

Table 2. Output performance and conversion efficiency of different types of TEGs.

Type of TEG	Improvement Measures	Temperature Difference	Output Power or Voltage	Conversion Efficiency	Ref.
L-Type	P-type and n-type thermal legs are designed with different heights	400 K	1.96 W	7.8%	[40]
X-Type	The cross-sectional area of the thermal leg gradually decreases from the upper and lower ends to the center	200 K	0.0847 W	5.2%	[41]

Table 2. *Cont.*

Type of TEG	Improvement Measures	Temperature Difference	Output Power or Voltage	Conversion Efficiency	Ref.
Asymmetric configuration	The cross-sectional area of the thermoelectric leg increases gradually along the direction of heat flow	-	76.66 W	1.45%	[42]
Two-stage TEG	Stack two layers of TEG	-	97.6 mV	3.9%	[43]
Two-stage TEG	Two layers of TEG are stacked, and different thermoelectric materials are used for hot end and cold-end TEG	300 K	-	6.89%	[44]
Segmented TEG	Bi_2Te_3/Skutteruditesegmented thermoelectric module	541 K	-	12%	[45]
Segmented TEG	Segmented annular TEG with double cone-shaped thermoelectric leg	-	-	-	[46]
Segmented TEG	Combining multiobjective genetic algorithm with finite element method	300 K	0.04326 W	9.63%	[47]

3. Micropower Supply

Due to the low power demand of microelectronic devices, thermoelectric power generation technology has broad application prospects in the field of micropower electronics. Thermoelectric micropower supplies include wearable thermoelectric devices that convert body heat into electricity, self-powered sensors, and microelectronics in the specific application environment.

3.1. Wearable Thermoelectric Devices

In recent years, with the rapid development of micro-nano processing technology and flexible electronic devices. The TEG can be integrated into wearable electronic devices owing to its miniaturization and flexible design, achieving self-powered energy collection of temperature differences between the human body and the environment. The current performance evaluation system for wearable TEG mainly focuses on two core indicators: output power density and wearing comfort. According to the differences in material systems and structural characteristics, wearable TEGs can be divided into two categories: traditional rigid TEGs represented by Bi_2Te_3, and flexible TEGs made of organic materials.

For the traditional rigid TEG, Nozariasbmarz et al. [48] studied the joint effect of material and device parameters on the efficiency of wearable TEG and developed a nanocomposite thermoelectric material based on Bi_2Te_3 (Figure 6a). The experimental results show that the power density of the nanocomposite TEG is 44 $\mu w \cdot cm^{-2}$ without airflow and can be increased to 156.5 $\mu w \cdot cm^{-2}$ under airflow, which is 4–7 times higher than that of similar commercial wearable TEG. Hyland et al. [49] proposed an efficient TEG design scheme for wearable applications and developed a functional T-shirt integrated with TEG (Figure 6b). By systematically measuring the power generation performance of TEG in different parts of the human body (such as the upper arm, forearm, chest, etc.), it is found that when TEG is installed in the upper arm, its output power reaches the maximum. Van et al. [50] realized TEG with high integration density through advanced assembly technology. The output power of the TEG reaches 91 μW at a 5 K temperature difference. Based on this technology, the research team successfully developed a wearable TEG prototype and verified the feasibility of its continuous power supply for electronic watches (Figure 6c). Van et al. [51] proposed a brain-computer system powered by wearable TEG (Figure 6d), with the output power of wearable TEG maintained at 2–2.5 mW (30 ± 2 $\mu w/cm^2$). However, due to the fixed geometry of the TEG based on Bi_2Te_3, they are difficult to fit the skin surface, resulting in low heat recovery efficiency. Organic thermoelectric materials have the advantage of flexible structure and can adapt to different shapes and sizes. Lv et al. [52] proposed a three-dimensional spring thermoelectric device with a basic double elastomer layer and air gap (Figure 6e). The device has excellent flexibility and compressibility, generating a power density of 416.22 nw/cm^2. Kim et al. [53] developed a self-powered wearable ECG system based on flexible PCB (Figure 6f). The system optimizes the performance of wearable TEG through a flexible radiator based on polymer so that its output power density reaches 38 $\mu w/cm^2$ in the initial 10 min and remains at 13 $\mu w/cm^2$ after 22 h of continuous operation so that it can continuously supply energy for ECG sensor and power management circuit. The aforemenioned research indicates that the flexible TEG of organic-inorganic composites enhances its bending (radius of curvature < 5 mm) and endows it with low thermal conductivity (<0.5 $w \cdot m^{-1} \cdot K^{-1}$), but its power density is usually lower than that of rigid wearable teg1-2 orders of magnitude.

Figure 6. (**i**) Nanocomposite thermoelectric materials based on Bi_2Te_3. "Reprinted with permission from Ref. [48]. 2020, Nozariasbmarz, A."; (**ii**) A T-shirt integrated with wearable TEG. "Reprinted with permission from Ref. [49]. 2016, Hyland, M."; (**iii**) Wearable TEG supplies power for electronic watches. "Reprinted with permission from Ref. [50]. 2021, Van Toan, N."; (**iv**) A brain-computer system powered by wearable TEG. "Reprinted with permission from Ref. [51]. 2008, Van Bavel, M."; (**v**) A three-dimensional spring thermoelectric device with basic double elastomer layer and air gap. "Reprinted with permission from Ref. [52]. 2021, Lv, H."; (**vi**) A self powered wearable ECG system based on flexible PCB. "Reprinted with permission from Ref. [53]. 2018, Kim, C.S."

3.2. Self-Powered Sensors

Automation and intelligence have become the development trend of modern industry. Thanks to this, intelligent sensors and microelectronics have made great development. More and more manufacturers incorporated sensors into products to improve their competitiveness. Current intelligent sensors and microelectronics require a few hundred microwatts or a few milliwatts of power to operate. Powering these devices typically requires extensive cabling from the battery, which often fails to satisfy the sensor's long-life demands. In some specific applications, sensors are required to work in extreme environments such as high temperature and vacuum. Wireless, long-life power supply, and extreme working environments are the main challenges that come to sensors. TEGs are an ideal candidate for these challenges. Beltrán et al. [54] proposed a TEG-powered vacuum pressure sensor and reported that the random error of the pressure signal was less than 10%. Kim et al. [55] designed a high-performance self-powered wireless sensor node powered by the flexible TEG, which can be used to remotely monitor the heat pipe temperature, ambient temperature, humidity, etc. Self-powered sensors and microelectronics are promising applications of TEGs. Guan et al. [56] developed a self-starting two-stage boost thermoelectric energy harvesting system, incorporating open-circuit voltage MPPT and low-power design; The system can self-start and efficiently supply power at an extremely low input of 20 mV/84 μW, driving microcontrollers and wireless sensors, with performance surpassing that of commercial solutions.

4. Thermoelectric Generator Systems from 1 W to 1 kW

At present, the output power of most TEG systems with preliminary application ranges from 1 W to 1 kW, including radiative TEG systems, solar thermoelectric generators, and automobile TEG systems. The recent developments, challenges, and prospects of these three TEG applications are discussed below.

4.1. Radiative Thermoelectric Generator System

In space exploration, satellites, and spacecraft require a long-term power supply to meet the needs of exploration missions. Current satellites and spacecraft are mainly powered by PV devices. However, due to the rotation of the planet, PV devices can receive sunlight for only half of the time at most, resulting in the deterioration of the lifespan of spacecraft. Radiative TEG systems utilize heat from natural radioactive decay as a power source. The exceptionally long half-lives of radioisotopes enable these systems to provide continuous electrical power for spacecraft over multi-decade timescales. In 1961, the PbTe-based radiative TEG system was first applied to the US Navy's Transit navigation satellite. The output power was about 2.7 W, but it operated for over fifteen years. Sponsored by NASA, radiative TEG systems with better performance have been developed continuously. In 1997, the Voyager I and II used 3 SiGe-based radiative TEG systems to provide 423 W of power for onboard electronics. This power is gradually reduced by about 7 W per year due to the decay of plutonium, and they are still in operation [57]. The success of radiative TEG systems developed by NASA has accelerated the application of thermoelectric power generation technology in space exploration, and an increasing number of countries have issued corresponding research plans.

4.2. Solar Application

Thermoelectric technology can also directly convert solar radiation into electricity based on the Seebeck effect. Unlike photovoltaic (PV) devices that directly convert light energy into electric energy, solar TEGs collect solar heat through a solar heat absorber and then transfer the heat to thermoelectric legs for power generation. Shittu et al. [58] analyzed the output performance of a segmented solar TEG through a numerical model and obtained that the output power was about 3 W under the radiation value of 11,000 W/m^2. Kraemer et al. [8] manufactured a skutterudite/Bi$_2$Te$_3$ segmented solar TEG and experimentally demonstrated its conversion efficiency under the direct normal irradiance of 211 kW/m^2. The experimental results showed that a peak efficiency of 7.4% was achieved. Cotfas et al. [59] prepared a metal oxide/additive composite absorption layer on the hot side of a solar TEG using spray deposition technology. The power generation increased by 25% under standard solar irradiance and by 82% under concentrated irradiance conditions. Cao et al. [60] proposed a solar TEG integrated with phase change materials and forced water cooling, achieving a power output of 6.42 mW and an output voltage of 307.3 mV at a solar irradiance of 1 kW/m², approximately 9 times higher than that of the traditional thermoelectric module (35.5 mV). Although the conversion efficiency of the solar TEG is still lower than that of PV devices, it is likely to become a promising alternative solar energy technology. However, the solar radiation in practical application is far lower than that in the laboratory. To be more competitive, the figure of merit of thermoelectric materials must be further improved. The high-performance heat absorber on the hot side of the solar TEG and the high-performance heat sink on the cold side of the solar TEG also help to improve its performance.

4.3. Automobile Thermoelectric Generator System

For automobile engines, about 1/3 of the thermal energy produced by burning fossil fuels is wasted in the form of waste heat with exhaust gas, resulting in serious energy waste and environmentally harmful emissions. The automobile thermoelectric generator (ATEG) system is considered a promising technology that can improve the fuel economy and reduce the use of fossil fuels. Automobile manufacturers and research institutes are trying to develop high-performance ATEG systems and integrate them into the vehicle exhaust system. However, the conversion efficiency of currently reported ATEG systems is about 2%, which seriously limits its wide commercial applications. Structure-based optimization is one of the most effective methods for improving the performance of ATEGs.

ATEGs primarily consist of heat exchangers (used to absorb heat from exhaust gases), thermoelectric modules (used to convert thermal energy into electrical energy), and radiators (used to maintain the cold-side temperature of the thermoelectric modules). The structural optimization of thermoelectric modules has been discussed in detail in Section 2.3. The optimization of the heat exchanger structure focuses primarily on enhancing its heat absorption efficiency. Luo et al. [61] proposed a convergent TEG (Figure 7a), which significantly enhanced the heat absorption efficiency of the heat exchanger, resulting in a 5.96% increase in the net output power of the TEG. To accommodate the circular exhaust pipe, Yang et al. [62] proposed a circular TEG with pin-fin type fins (Figure 7b) and determined the optimal structure of the TEG using Taguchi optimization; The net power reached

34.11 W, representing an 18.7% increase compared to the original design. Studies have shown that the installation of fins inside the heat exchanger can significantly enhance its heat absorption efficiency. Consequently, researchers aim to optimize the fin structure. Luo et al. [63] proposed a fin with dimples based on plate fins (Figure 7c) and determined the optimal design of the dimples through numerical simulations. The net output power increased by 10.09%. Ge et al. [64] introduced twisted-strip fins into the heat exchanger and optimized their pitch ratio, twist ratio, and tilt angle (Figure 7d), resulting in a 30% increase in the output power of the TEG.

Additionally, heat pipes exhibit exceptional heat transfer performance, fully meeting the high thermal conductivity requirements of ATEGs. Luo et al. [65] proposed a novel ATEG integrated with heat pipes, introducing the heat pipes into the heat exchanger (Figure 7e). The incorporation of heat pipes expanded the thermal side area of the heat exchanger, resulting in an output power of 213.19 W, representing a 42.95% increase. Pacheco et al. [66] longitudinally installed heat pipes inside the heat exchanger, significantly enhancing the temperature uniformity of the exchanger due to the high thermal conductivity of the heat pipes. Despite the promising results of the aforementioned studies, the generated electrical power remains insufficient to fully meet the power supply requirements of the vehicle. To achieve higher output power, a larger ATEG is necessary. To address this, Liu et al. [67] integrated four identical ATEGs in parallel into a vehicle (Figure 7f), achieving a maximum output power of 944 W in the tests. Zhang et al. [68] stacked multiple small heat exchangers together (Figure 7g), resulting in a maximum output power of 1002.6 W for the TEG, although this also resulted in a high-pressure drop. Although these large ATEGs generate exceptionally high output power, they occupy a significant portion of the vehicle's space. Therefore, maximizing the output power of ATEGs within limited space is an important research endeavor for future development.
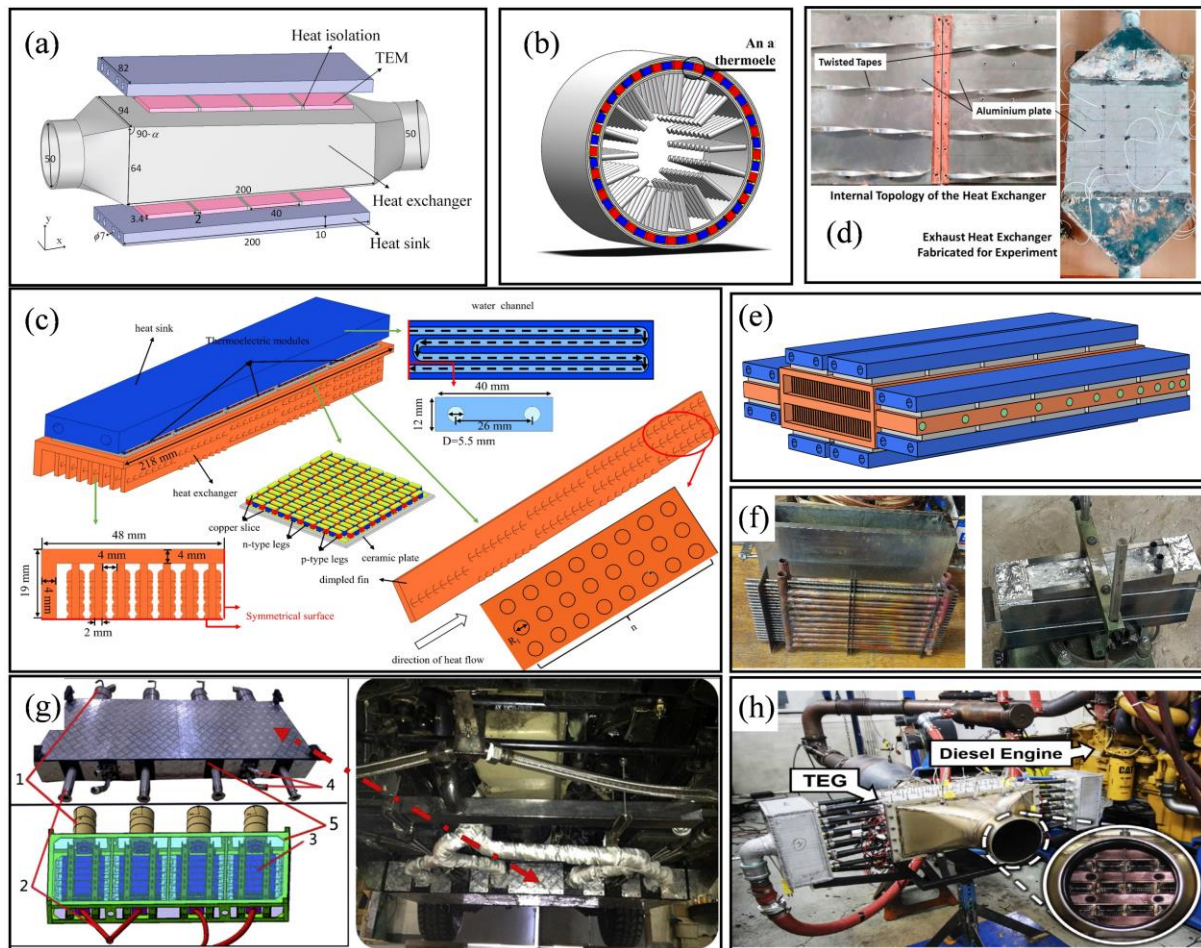

Figure 7. (**a**) Convergent TEG. "Reprinted with permission from Ref. [61]. 2019, Luo, D."; (**b**) Pin-fin type circular TEG. "Reprinted with permission from Ref. [62]. 2024, Yang, W."; (**c**) Fins with dimples. "Reprinted with permission from Ref. [63]. 2024, Luo, D."; (**d**) TEG with twisted band fins. "Reprinted with permission from Ref. [64]. 2025, Ge, M."; (**e**) Expand the hot side area of the heat exchanger using heat pipes. "Reprinted with permission from Ref. [65]. 2024, Luo, D."; (**f**) Using heat pipes to improve the temperature uniformity of heat exchangers. "Reprinted with permission from Ref. [66]. 2020, Pacheco, N."; (**g**) Four-TEG system. "Reprinted with permission from Ref. [67]. 2015, Liu, X."; (**h**) Compact TEG. "Reprinted with permission from Ref. [68]. 2015, Zhang, Y.".

5. Thermoelectric Generator Systems Exceed 1 kW

In addition to recycling the waste heat in automobile exhaust, TEG can also be applied to the recovery of waste heat from ships and industrial waste gases. The exhaust gas temperature in these fields is usually high and the waste heat is huge. Therefore, the power generation capacity of TEG system in these application scenarios often exceeds 1 kW and even can achieve higher power output.

In ship application, TEG can recover heat energy from high-temperature exhaust gas emitted by the engine and further improve energy recovery efficiency by using other waste heat sources generated during ship operation, such as boiler exhaust gas and engine room waste heat. This waste heat recovery system can provide clean power for ships, reduce dependence on traditional generators, and effectively reduce fuel consumption and improve the overall energy efficiency of ships. Compared with TEGs applied to vehicles, the TEG system applied to ships can ignore the negative impact of increased weight. However, few studies have been perfomed to develop whole TEG system prototypes for ship waste heat recovery because it requires a large number of TEG modules and costs. Georgopoulou et al. [69] studied the waste heat recovery potential of TEGs for marine applications, and results showed that the installation of TEGs could generate about 26 kW of extra power, corresponding to 0.2% of the main engine power. Eddine et al. [16] analyzed and optimized the performance of a simplified ship TEG system through a theoretical model. Results showed that the Bi_2Te_3-based TEG module was more suitable for ship waste heat recovery, and its output power was 70% higher than that of the SiGe-based TEG. With the increasing demand for fuel economy, ship manufacturers are opting to utilize TEGs to optimize ship waste heat recovery, because it has a weight advantage, offers a free cooling source, and does not require maintenance.

In the industrial field, especially in high-temperature industrial processes (such as metallurgy, chemical industry, glass production, etc.), the TEG system can effectively extract heat energy generated from the high-temperature exhaust gases. TEG can achieve high power output by optimizing the heat exchange system and thermoelectric materials. In industrial waste heat recovery, technologies, such as the organic Rankine cycle, steam turbines, and Stirling engines, are increasingly being optimized. As a promising energy technology, various waste heat projects using TEGs have been studied. Luo et al. [15] proposed a novel TEG system to harvest waste heat from cement rotary kilns, in which 3480 Bi_2Te_3–PbTe TEG modules were applied on the walls of the kiln. The system performance was estimated using a mathematical model. Results showed that the system can produce about 211 kW of electrical power and recover more than 32.85% of the heat that used to be lost as waste heat through the kiln surface. Kuroki et al. [70] described a TEG system used for waste heat recovery in the steelmaking industry, which contains 896 Bi_2Te_3-based TEG modules. Experimental results showed that the system could generate 9 kW electricity when the slab temperature was about 1188 K and the slab width was 1.7 m. Although the conversion efficiency of the TEG system is low (~2%), it still enables considerable application prospects in the field of industrial waste heat recovery. The cost of installing TEG systems will be recovered within a few years because the furnace works 24 h a day.

Looking forward to the future, the application potential of TEG technology in the field of industrial waste heat recovery is still huge. With the continuous progress of thermoelectric materials, heat exchange technology, and system optimization design, the efficiency and output power of the TEG system need to be further optimized. In addition, with the increasing demand for energy conservation and environmental protection in the market, TEG, as a green and low-carbon energy recovery technology, is expected to be increasingly applied in industrial waste heat recovery, ship energy recovery, and other high-temperature waste gas utilization.

6. Conclusions

In this review, basic principles, recent advances, current challenges, and prospects of thermoelectric power generation from micropower supplies to kilowatt systems are discussed. As a basic power unit of the TEG system, the performance of the TEG module can be improved by applying high-performance thermoelectric materials and advanced structural design. For micropower supplies, the wearable TEG system should not only pay attention to performance improvement but also comfort, while the self-powered sensors and microelectronics mainly focus on the performance and application environment. For TEG systems from 1 W to 1 kW, preliminary applications have been achieved, such as radiative, stove, and automobile TEG systems, among which the automobile TEG system has the potential to generate over 1 kW of electricity. When TEGs are applied to waste heat recovery from the ship and industrial exhaust gas, the TEG system can easily generate an output power of more than 1 kW, and there is an increasing interest in using TEGs to reduce energy use. Ongoing developments in thermoelectric materials and devices will soon facilitate broader adoption of thermoelectric power generation technologies.

Despite these advancements, critical challenges persist in TEG applications, including inherent limitations in thermoelectric material efficiency (e.g., low *ZT* values at mid-to-low temperature ranges), interfacial thermal

resistance in system integration, and long-term stability under cyclic thermal stresses. Future studies should investigate nanostructured composites and topology-optimized modules to decouple electronic and thermal transport properties, as well as AI-driven design frameworks for hybrid energy systems. Emerging applications in IoT power supply and aerospace waste heat recovery, coupled with scalable manufacturing techniques like inkjet printing of thermoelectric films, are expected to accelerate the transition of TEGs from niche applications to industrial ubiquity.

References

1. Ge, M.; Li, Z.; Wang, Y.; et al. Experimental study on thermoelectric power generation based on cryogenic liquid cold energy. *Energy* **2021**, *220*, 119746. https://doi.org/10.1016/j.energy.2020.119746.

2. Luo, D.; Yu, Y.; Yan, Y.; et al. Increasing power densities in a thermoelectric generator by stacking and incorporating dual heat pipes. *Device* **2024**, *2*, 100435. https://doi.org/10.1016/j.device.2024.100435.

3. Luo, D.; Liu, Z.; Cao, J.; et al. Feasibility and parametric study of a groove-type thermoelectric generator under multiphysics field conditions. *Appl. Therm. Eng.* **2025**, *259*, 124972. https://doi.org/10.1016/j.applthermaleng.2024.124972.

4. Luo, D.; Wu, Z.; Zhang, Z.; et al. Transient thermal analysis of a thermoelectric-based battery thermal management system at high temperatures. *Energy* **2025**, *318*, 134833. https://doi.org/10.1016/j.energy.2025.134833.

5. He, T.; Nair, S.K.; Babu, P.; et al. A novel conceptual design of hydrate based desalination (HyDesal) process by utilizing LNG cold energy. *Appl. Energy* **2018**, *222*, 13–24. https://doi.org/10.1016/j.apenergy.2018.04.006.

6. Shih, W.-C.; Matsuda, M.; Konno, K.; et al. Tailored thermoelectric performance of poly(phenylene butadiynylene)s/carbon nanotubes nanocomposites towards wearable thermoelectric generator application. *Compos. Part B Eng.* **2024**, *286*, 111779. https://doi.org/10.1016/j.compositesb.2024.111779.

7. Bennett, G. Space Nuclear Power: Opening the Final Frontier. In Proceedings of the 4th International Energy Conversion Engineering Conference and Exhibit (IECEC), San Diego, CA, USA, 26–29 June 2006.

8. Kraemer, D.; Jie, Q.; McEnaney, K.; et al. Concentrating solar thermoelectric generators with a peak efficiency of 7.4%. *Nat. Energy* **2016**, *1*, 16153. https://doi.org/10.1038/nenergy.2016.153.

9. Zhao, R.; Zhu, N.; Zhao, X.; et al. Multi-objective optimization of a novel photovoltaic-thermoelectric generator system based on hybrid enhanced algorithm. *Energy* **2025**, *319*, 135046. https://doi.org/10.1016/j.energy.2025.135046.

10. Suresh Prasanna, C.; Harish, S.; Archana, J.; et al. Interfacial energy barrier tuning in MnO_2/MoS_2/Carbon fabric integrated with low resistance textrode for highly efficient wearable thermoelectric generator. *Carbon* **2024**, *218*, 118609. https://doi.org/10.1016/j.carbon.2023.118609.

11. Luo, D.; Li, Z.; Yang, S.; et al. Improved performance of the thermoelectric generator by combining vapor chambers and circular fins. *Energy* **2025**, *320*, 135354. https://doi.org/10.1016/j.energy.2025.135354.

12. Luo, D.; Yang, S.; Li, Z.; et al. Transient energy, exergy, and economic analysis of an automotive thermoelectric generator with different structures. *Appl. Energy* **2025**, *377*, 124494. https://doi.org/10.1016/j.apenergy.2024.124494.

13. Luo, D.; Yang, S.; Zhang, H.; et al. Performance improvement of an automotive thermoelectric generator by introducing a novel split fin structure. *Appl. Energy* **2025**, *382*, 125218. https://doi.org/10.1016/j.apenergy.2024.125218.

14. Yang, S.; Chen, H.; Yang, X.; et al. Design optimization of split fins in heat pipe-based thermoelectric generators. *Energy* **2025**, *322*, 135547. https://doi.org/10.1016/j.energy.2025.135547.

15. Luo, Q.; Li, P.; Cai, L.; et al. A Thermoelectric Waste-Heat-Recovery System for Portland Cement Rotary Kilns. *J. Electron. Mater.* **2015**, *44*, 1750–1762. https://doi.org/10.1007/s11664-014-3543-1.

16. Nour Eddine, A.; Chalet, D.; Faure, X.; et al. Optimization and characterization of a thermoelectric generator prototype for marine engine application. *Energy* **2018**, *143*, 682–695. https://doi.org/10.1016/j.energy.2017.11.018.

17. Miao, Z.; Meng, X.; Li, X. Design a high-performance thermoelectric generator by analyzing industrial heat transfer. *Appl. Energy* **2023**, *347*, 121403. https://doi.org/10.1016/j.apenergy.2023.121403.

18. Liu, X.; Wang, K.; Shen, Z. A novel strategy of inserting radiation shields to enhance the performance of thermoelectric generator systems for industrial high-temperature heat recovery. *Energy* **2024**, *301*, 131704. https://doi.org/10.1016/j.energy.2024.131704.

19. Luo, D.; Wang, R.C. Experimental Test and Estimation of the Equivalent Thermoelectric Properties for a Thermoelectric Module. *J. Energy Resour. Technol.-Trans. Asme* **2021**, *143*, 122102. https://doi.org/10.1115/1.4050132.

20. Luo, D.; Chen, H.; Chen, W.-H.; et al. Interdependent optimization strategies for material, module, and system designs in thermoelectric devices. *Device* **2025**, 100752. https://doi.org/10.1016/j.device.2025.100752.

21. Bell, L.E. Cooling, Heating, Generating Power, and Recovering Waste Heat with Thermoelectric Systems. *Science* **2008**, *321*, 1457. https://doi.org/10.1126/science.1158899.

22. Twaha, S.; Zhu, J.; Yan, Y.; et al. A comprehensive review of thermoelectric technology: Materials, applications, modelling and performance improvement. *Renew. Sustain. Energy Rev.* **2016**, *65*, 698–726. https://doi.org/10.1016/j.rser.2016.07.034.

23. Zheng, X.F.; Liu, C.X.; Yan, Y.Y.; et al. A review of thermoelectrics research—Recent developments and potentials for sustainable and renewable energy applications. *Renew. Sustain. Energy Rev.* **2014**, *32*, 486–503. https://doi.org/10.1016/j.rser.2013.12.053.

24. Luo, D.; Wang, R.; Yu, W.; et al. Parametric study of a thermoelectric module used for both power generation and cooling. *Renew. Energy* **2020**, *154*, 542–552. https://doi.org/10.1016/j.renene.2020.03.045.

25. Wu, Y.; Ma, W.; Guo, Z.-Y. Governing equations of thermoelectric generators. *Int. J. Heat Mass Transf.* **2025**, *241*, 126737. https://doi.org/10.1016/j.ijheatmasstransfer.2025.126737.

26. Luo, D.; Wang, R.; Yu, W. Comparison and parametric study of two theoretical modeling approaches based on an air-to-water thermoelectric generator system. *J. Power Sources* **2019**, *439*, 227069. https://doi.org/10.1016/j.jpowsour.2019.227069.

27. Siddique, A.R.M.; Mahmud, S.; Heyst, B.V. A review of the state of the science on wearable thermoelectric power generators (TEGs) and their existing challenges. *Renew. Sustain. Energy Rev.* **2017**, *73*, 730–744. https://doi.org/10.1016/j.rser.2017.01.177.

28. Ma, Y.; Hao, Q.; Poudel, B.; et al. Enhanced Thermoelectric Figure-of-Merit in p-Type Nanostructured Bismuth Antimony Tellurium Alloys Made from Elemental Chunks. *Nano Lett.* **2008**, *8*, 2580–2584. https://doi.org/10.1021/nl8009928.

29. Ohta, M.; Biswas, K.; Lo, S.-H.; et al. Enhancement of Thermoelectric Figure of Merit by the Insertion of MgTe Nanostructures in p-type PbTe Doped with Na_2Te. *Adv. Energy Mater.* **2012**, *2*, 1117–1123. https://doi.org/10.1002/aenm.201100756.

30. Joshi, G.; Lee, H.; Lan, Y.; et al. Enhanced Thermoelectric Figure-of-Merit in Nanostructured p-type Silicon Germanium Bulk Alloys. *Nano Lett.* **2008**, *8*, 4670–4674. https://doi.org/10.1021/nl8026795.

31. Kim, S.I.; Lee, K.H.; Mun, H.A.; et al. Dense dislocation arrays embedded in grain boundaries for high-performance bulk thermoelectrics. *Science* **2015**, *348*, 109–114. https://doi.org/10.1126/science.aaa4166.

32. Wang, Y.; Liu, W.-D.; Shi, X.-L.; et al. Enhanced thermoelectric properties of nanostructured n-type Bi_2Te_3 by suppressing Te vacancy through non-equilibrium fast reaction. *Chem. Eng. J.* **2020**, *391*, 123513. https://doi.org/10.1016/j.cej.2019.123513.

33. Meroz, O.; Elkabets, N.; Gelbstein, Y. Enhanced Thermoelectric Properties of n-Type Bi_2Te_3–xSex Alloys following Melt-Spinning. *ACS Appl. Energy Mater.* **2020**, *3*, 2090–2095. https://doi.org/10.1021/acsaem.9b02133.

34. Zheng, Y.; Liu, C.; Miao, L.; et al. Extraordinary thermoelectric performance in MgAgSb alloy with ultralow thermal conductivity. *Nano Energy* **2019**, *59*, 311–320. https://doi.org/10.1016/j.nanoen.2019.02.045.

35. Wu, Y.; Chen, Z.; Nan, P.; et al. Lattice Strain Advances Thermoelectrics. *Joule* **2019**, *3*, 1276–1288. https://doi.org/10.1016/j.joule.2019.02.008.

36. Rogl, G.; Grytsiv, A.; Rogl, P.; et al. n-Type skutterudites (R,Ba,Yb)yCo$_4$Sb$_{12}$ (R = Sr, La, Mm, DD, SrMm, SrDD) approaching ZT ≈ 2.0. *Acta Mater.* **2014**, *63*, 30–43. https://doi.org/10.1016/j.actamat.2013.09.039.

37. Tsai, Y.-F.; Wei, P.-C.; Chang, L.; et al. Compositional Fluctuations Locked by Athermal Transformation Yielding High Thermoelectric Performance in GeTe. *Adv. Mater.* **2021**, *33*, 2005612. https://doi.org/10.1002/adma.202005612.

38. Saiga, Y.; Du, B.; Deng, S.K.; et al. Thermoelectric properties of type-VIII clathrate Ba8Ga16Sn30 doped with Cu. *J. Alloys Compd.* **2012**, *537*, 303–307. https://doi.org/10.1016/j.jallcom.2012.05.049.

39. Shi, X.; Zhao, T.; Zhang, X.; et al. Extraordinary n-Type Mg$_3$SbBi Thermoelectrics Enabled by Yttrium Doping. *Adv. Mater.* **2019**, *31*, 1903387. https://doi.org/10.1002/adma.201903387.

40. Luo, D.; Liu, Z.; Cao, J.; et al. Performance investigation and optimization of an L-type thermoelectric generator. *Energy* **2024**, *307*, 132768. https://doi.org/10.1016/j.energy.2024.132768.

41. Wang, R.; Meng, Z.; Luo, D.; et al. A Comprehensive Study on X-Type Thermoelectric Generator Modules. *J. Electron. Mater.* **2020**, *49*, 4343–4354. https://doi.org/10.1007/s11664-020-08152-4.

42. Luo, D.; Zhang, H.; Cao, J.; et al. Innovative design of an annular thermoelectric generator for enhanced automotive waste heat recovery. *Energy Convers. Manag.* **2024**, *313*, 118584. https://doi.org/10.1016/j.enconman.2024.118584.

43. de Oca, O.Y.E.-M.; Olivares-Robles, M.A. Dynamic performance optimization of two-stage thermoelectric generator: Impact of different geometric leg shapes in each stage. *Energy Rep.* **2024**, *11*, 597–610. https://doi.org/10.1016/j.egyr.2023.12.032.

44. Bian, M.; Xu, Z.; Tang, X.; et al. Tri-objective and multi-parameter geometric optimization of two-stage radioisotope thermoelectric generator based on NSGA-II. *Appl. Therm. Eng.* **2025**, *258*, 124685. https://doi.org/10.1016/j.applthermaleng.2024.124685.

45. Zhang, Q.; Liao, J.; Tang, Y.; et al. Realizing a thermoelectric conversion efficiency of 12% in bismuth telluride/skutterudite segmented modules through full-parameter optimization and energy-loss minimized integration. *Energy Environ. Sci.* **2017**, *10*, 956–963. https://doi.org/10.1039/C7EE00447H.

46. He, H.; Xie, Y.; Zuo, Q.; et al. Optimization analysis for thermoelectric performance improvement of biconical segmented annular thermoelectric generator. *Energy* **2024**, *306*, 132397. https://doi.org/10.1016/j.energy.2024.132397.

47. Sun, Y.; Zhai, P.; Wang, S.; et al. Performance enhancement of segmented annular thermoelectric generator based on multi-parameter and multi-objective optimization. *Therm. Sci. Eng. Prog.* **2024**, *47*, 102245. https://doi.org/10.1016/j.tsep.2023.102245.

48. Nozariasbmarz, A.; Suarez, F.; Dycus, J.H.; et al. Thermoelectric generators for wearable body heat harvesting: Material and device concurrent optimization. *Nano Energy* **2020**, *67*, 104265. https://doi.org/10.1016/j.nanoen.2019.104265.

49. Hyland, M.; Hunter, H.; Liu, J.; et al. Wearable thermoelectric generators for human body heat harvesting. *Appl. Energy* **2016**, *182*, 518–524. https://doi.org/10.1016/j.apenergy.2016.08.150.

50. Van Toan, N.; Thi Kim Tuoi, T.; Van Hieu, N.; et al. Thermoelectric generator with a high integration density for portable and wearable self-powered electronic devices. *Energy Convers. Manag.* **2021**, *245*, 114571. https://doi.org/10.1016/j.enconman.2021.114571.

51. Van Bavel, M.; Leonov, V.; Yazicioglu, R.F.; et al. Wearable battery-free wireless 2-channel EEG systems powerd by energy scavengers. *Sens. Transducers J.* **2008**, *94*.

52. Lv, H.; Liang, L.; Zhang, Y.; et al. A flexible spring-shaped architecture with optimized thermal design for wearable thermoelectric energy harvesting. *Nano Energy* **2021**, *88*, 106260. https://doi.org/10.1016/j.nanoen.2021.106260.

53. Kim, C.S.; Yang, H.M.; Lee, J.; et al. Self-Powered Wearable Electrocardiography Using a Wearable Thermoelectric Power Generator. *ACS Energy Lett.* **2018**, *3*, 501–507. https://doi.org/10.1021/acsenergylett.7b01237.

54. Beltrán-Pitarch, B.; García-Cañadas, J. A novel vacuum pressure sensor using a thermoelectric device. *Vacuum* **2020**, *172*, 109088. https://doi.org/10.1016/j.vacuum.2019.109088.

55. Kim, Y.J.; Gu, H.M.; Kim, C.S.; et al. High-performance self-powered wireless sensor node driven by a flexible thermoelectric generator. *Energy* **2018**, *162*, 526–533. https://doi.org/10.1016/j.energy.2018.08.064.

56. Guan, M.; Wang, K.; Xu, D.; et al. Design and experimental investigation of a low-voltage thermoelectric energy harvesting system for wireless sensor nodes. *Energy Convers. Manag.* **2017**, *138*, 30–37. https://doi.org/10.1016/j.enconman.2017.01.049.

57. Champier, D. Thermoelectric generators: A review of applications. *Energy Convers. Manag.* **2017**, *140*, 167–181. https://doi.org/10.1016/j.enconman.2017.02.070.

58. Shittu, S.; Li, G.; Xuan, Q.; et al. Electrical and mechanical analysis of a segmented solar thermoelectric generator under non-uniform heat flux. *Energy* **2020**, *199*, 117433. https://doi.org/10.1016/j.energy.2020.117433.

59. Cotfas, D.T.; Enesca, A.; Cotfas, P.A. Enhancing the performance of the solar thermoelectric generator in unconcentrated and concentrated light. *Renew. Energy* **2024**, *221*, 119831. https://doi.org/10.1016/j.renene.2023.119831.

60. Cao, Z.; Li, W. A day-night solar thermoelectric generator enabled by phase change material and forced water cooling. *Sol. Energy* **2024**, *268*, 112315. https://doi.org/10.1016/j.solener.2024.112315.

61. Luo, D.; Wang, R.; Yu, W.; et al. Modelling and simulation study of a converging thermoelectric generator for engine waste heat recovery. *Appl. Therm. Eng.* **2019**, *153*, 837–847. https://doi.org/10.1016/j.applthermaleng.2019.03.060.

62. Yang, W.; Jin, C.; Zhu, W.; et al. Taguchi optimization and thermoelectrical analysis of a pin fin annular thermoelectric generator for automotive waste heat recovery. *Renew. Energy* **2024**, *220*, 119628. https://doi.org/10.1016/j.renene.2023.119628.

63. Luo, D.; Li, Z.; Yan, Y.; et al. Design and optimization of a thermoelectric generator with dimple fins to achieve higher net power. *Appl. Therm. Eng.* **2024**, *252*, 123735. https://doi.org/10.1016/j.applthermaleng.2024.123735.

64. Ge, M.; Zhao, C.; Xiao, Y.; et al. Experimental study on enhancing thermoelectric performance of exhaust thermoelectric generator using multi-orifice plate. *J. Clean. Prod.* **2025**, *486*, 144446. https://doi.org/10.1016/j.jclepro.2024.144446.

65. Luo, D.; Yang, S.; Yan, Y.; et al. Performance improvement of the automotive thermoelectric generator by extending the hot side area of the heat exchanger through heat pipes. *Energy Convers. Manag.* **2024**, *310*, 118472. https://doi.org/10.1016/j.enconman.2024.118472.

66. Pacheco, N.; Brito, F.P.; Vieira, R.; et al. Compact automotive thermoelectric generator with embedded heat pipes for thermal control. *Energy* **2020**, *197*, 117154. https://doi.org/10.1016/j.energy.2020.117154.

67. Liu, X.; Deng, Y.D.; Li, Z.; et al. Performance analysis of a waste heat recovery thermoelectric generation system for automotive application. *Energy Convers. Manag.* **2015**, *90*, 121–127. https://doi.org/10.1016/j.enconman.2014.11.015.

68. Zhang, Y.; Cleary, M.; Wang, X.; et al. High-temperature and high-power-density nanostructured thermoelectric generator for automotive waste heat recovery. *Energy Convers. Manag.* **2015**, *105*, 946–950. https://doi.org/10.1016/j.enconman.2015.08.051.

69. Georgopoulou, C.A.; Dimopoulos, G.G.; Kakalis, N.M.P. A modular dynamic mathematical model of thermoelectric elements for marine applications. *Energy* **2016**, *94*, 13–28. https://doi.org/10.1016/j.energy.2015.10.130.

70. Kuroki, T.; Kabeya, K.; Makino, K.; et al. Thermoelectric Generation Using Waste Heat in Steel Works. *J. Electron. Mater.* **2014**, *43*, 2405–2410. https://doi.org/10.1007/s11664-014-3094-5.